Downscaling and Projection of Winter Extreme Daily Precipitation over North America

JIAFENG WANG AND XUEBIN ZHANG

Climate Research Division, Environment Canada, Toronto, Ontario, Canada

(Manuscript received 11 September 2006, in final form 20 July 2007)

ABSTRACT

Large-scale atmospheric variables have been statistically downscaled to derive winter (December–March) maximum daily precipitation at stations over North America using the generalized extreme value distribution (GEV). Here, the leading principal components of the sea level pressure field and local specific humidity are covariates of the distribution parameters. The GEV parameters are estimated using data from 1949 to 1999 and the *r*-largest method. This statistical downscaling procedure is found to yield skill over the southern and northern West Coast, central United States, and areas of western and eastern Canada when tested with independent data.

The projected changes in covariates or predictors are obtained from transient climate change simulations conducted with the Canadian Centre for Climate Modelling and Analysis (CCCma) Coupled General Circulation Model, version 3.1 (CGCM3.1) forced by the Intergovernmental Panel on Climate Change (IPCC) A2 forcing scenario. They are then used to derive the GEV distribution parameters for the period 2050–99. The projected frequency of the current 20-yr return maximum daily precipitation for that period suggests that extreme precipitation risk will increase heavily over the south and central United States but decrease over the Canadian prairies. The difference between the statistical downscaling results and those estimated using GCM simulation is also discussed.

1. Introduction

Changes in extreme precipitation due to the increase in greenhouse gases in the atmosphere have received increasing attention. This is because extreme precipitation can be more variable than total precipitation (Groisman et al. 1999; Katz 1999), and it is extreme precipitation that has greater potential to result in natural disasters (Meehl et al. 2000). In addition, general circulation model (GCM) simulations suggest that extreme precipitation will change at a much greater rate than the total precipitation in the future (Zwiers and Kharin 1998; Kharin and Zwiers 2000; Kharin et al. 2007). Plausible scenarios are required to assess extreme precipitation change impacts. Scenarios at local scale and resolution finer than GCM resolution may be produced with regional climate models. For example, Bell et al. (2004) used regional climate model simulations to construct extreme climate scenarios for California. This dynamical downscaling approach provides output at a resolution much higher than a GCM can produce, but at a very high computational cost. An alternative approach is to make use of statistical tools, typically regression methods, by establishing a statistical relationship between local-scale variables and GCM-simulated large-scale fields. Such a statistical downscaling approach has an advantage of being easy and inexpensive to use and easy to understand. It has been used in many studies to construct regional climate scenarios over North America (e.g., Wigley et al. 1990; Crane and Hewitson 1998; Easterling 1999). Because of the importance of extreme precipitation, some studies have also attempted to derive scenarios for extreme precipitation from large-scale fields. Cavazos (1999) used an artificial neural network (ANN) technique to downscale daily rainfall in the winter season for northeastern Mexico and southeastern Texas from a circulation–humidity field. He found that his method was successful in differentiating the driest from wettest winters, but wet winters' extreme precipitation amount was not well reproduced. Harpham and Wilby (2005) compared

Corresponding author address: Dr. Xuebin Zhang, CRD, Environment Canada, 4905 Dufferin Street, Toronto, ON M3H 5T4, Canada.
E-mail: xuebin.zhang@ec.gc.ca

DOI: 10.1175/2007JCLI1671.1

three statistical models for downscaling occurrences and amounts of heavy daily precipitation at multiple sites. They found that the aggregation of dry and wet days was well reproduced, but the skill for reproducing annual quantiles and exceedance thresholds was poor. Schmidli et al. (2007) compared daily precipitation statistics obtained by using six statistical and three dynamical downscaling models for the European Alps. They found that the performance for reproducing the present climate conditions varied substantially for different regions and/or seasons. They also found that the skill of downscaling precipitation-intensity-related indices is generally lower than that of precipitation occurrence. These studies have focused on moderate extremes at their best. None of them have attempted to downscale maximum daily precipitation amount, which is very relevant to many impact studies, directly from the large-scale field. This is the main focus of the current paper.

A typical statistical downscaling method uses some sort of regression method that assumes that the downscaled variables have normal probability distributions. It is, in general, not suitable for downscaling extreme precipitation since extreme precipitation follows a form of generalized extreme value distribution (GEV). To address this issue, Katz et al. (2002) proposed a method that uses the GEV distribution whose parameters are functions of predictors (e.g., sea level pressure, ENSO index, etc.). This idea has been further extended to the development of methods for producing future scenarios of extreme wave height for the North Atlantic Ocean (Wang et al. 2004) and for computing trends in extreme values (Zhang et al. 2004). Wang et al. (2004) found that the use of seasonal mean sea level pressure (SLP) anomaly and squared SLP gradient index as covariates can significantly improve the goodness-of-fit of significant wave heights over the North Atlantic Ocean, meaning that these variables have significant influence on the wave weights. As a result, they used the empirical relationship between large-scale predictors and local wave heights and model-projected future scenarios of the predictors to produce future projections of extreme wave height. Zhang et al. (2004) found that the power of detecting a significant trend in extreme values is improved if the underlining probability distribution of extreme values is considered. They also suggested the use of the *r*-largest method, that is, using the *r*-largest values rather than the single largest value in a season or a year, which potentially makes more efficient use of data for model fitting to improve the power.

This study presents a method for construction of an extreme precipitation scenario over North America using a statistical downscaling approach. We improve the approach in Wang et al. (2004) by using the *r*-largest method to establish a statistical relationship between large-scale predictors and winter season maximum daily precipitation at a station. Independent data have been used to validate the downscaling procedure. We then use projected changes in predictors extracted from GCM simulations to derive parameters of GEV distributions corresponding to the last 50 yr of the twenty-first century, and subsequently to estimate the changes in the risk of extreme precipitation. The remainder of this paper is organized as follows: the methods and data are described in sections 2 and 3, respectively; results are presented in section 4; and a summary and discussion are given in section 5.

2. Methods

A statistical downscaling approach requires two basic ingredients: 1) a proper regression model that establishes the connection between predictors and the predictand statistically, and 2) predictor variables that have a strong influence on the predictand. When constructing scenarios for the future, it is also assumed that the observed statistical relationship is still valid for the future and the predictors are well simulated by the GCM. In the following, our statistical methods are briefly outlined.

a. Modeling the extreme value distribution

Extreme daily precipitation may be modeled with a GEV distribution whose cumulative distribution function has the following form:

$$F(y) = \begin{cases} \exp\{-[1 + \xi(y - \mu)/\sigma]^{-1/\xi}\}, & 1 + \xi(y - \mu)/\sigma > 0, \quad \xi \neq 0, \\ \exp\{-\exp[-(y - \mu)/\sigma]\}, & \xi = 0, \end{cases} \tag{1}$$

where μ, $\sigma(>0)$, and ξ are the location, scale, and shape parameters, respectively. Predictor variables may be incorporated into the GEV distribution (e.g., Smith 1989; Coles 2001; Katz et al. 2002) by expressing the location and scale parameters as functions of the predictors. The shape parameter is usually taken as a constant. Because the scale parameter needs to be positive, a log transferred scale parameter is used:

$$\begin{cases} \mu = \mu_0 + \sum_{j=1}^{J} a_j x_j \\ \ln(\sigma) = \sigma_0 + \sum_{j=1}^{J} b_j x_j \\ \xi = \xi_0 \end{cases}, \tag{2}$$

where $x_1, x_2, \cdots x_J$ are J predictor variables. In the following, we call the model without a predictor (the caes when $J = 0$) M_0. In this case, the covariates have no influence on the parameters of the distribution, and the modeling becomes the classical GEV modeling. The coefficients a_j, b_j, $(j = 1, 2, \cdots, J)$ represent the effect of predictors on the GEV distribution. They can be estimated using the maximum likelihood (ML) method, along with μ_0, σ_0, and ξ_0.

Instead of using one largest value for each winter, we use the $r(r > 1)$ top values. This approach makes better use of information in the daily data and reduces the uncertainty in parameter estimation. The method is called the r-largest method (Coles 2001) in the statistical literature. When r largest values are used, the likelihood function becomes

$$L(\mu, \sigma, \xi) = \prod_{i=1}^{m} \left\langle \exp\left\{ -\left[1 + \xi\left(\frac{y_i^{(r)} - \mu}{\sigma} \right) \right]^{-(1/\xi)} \right\} \times \prod_{k=1}^{r} \sigma^{-1} \left[1 + \xi\left(\frac{y_i^{(k)} - \mu}{\sigma} \right) \right]^{-(1/\xi)-1} \right\rangle, \tag{3}$$

where $y_i^{(k)}(i = 1, 2, \cdots, m; k = 1, 2, \cdots, r)$ is the kth largest precipitation amount in the winter i, and m is the number of winters. The choice of r is a compromise between uncertainty and bias (see Zhang et al. 2004 for details): a larger r uses more information and hence helps to reduce uncertainty in parameter estimation; but on the other hand, a larger r also increases biases in the estimation due to the use of smaller extreme values. The likelihood ratio test (described below) indicates that wintertime maximum daily precipitation amount over North America can generally be modeled with a Gumbel distribution, a special case of GEV where $\xi = 0$. In this case, the likelihood function of (3) becomes

$$L(\mu, \sigma) = \prod_{i=1}^{m} \left\langle \exp\left\{ -\exp\left[-\left(\frac{y_i^{(r)} - \mu}{\sigma} \right) \right] \right\} \times \prod_{k=1}^{r} \sigma^{-1} \exp\left[-\left(\frac{y_i^{(k)} - \mu}{\sigma} \right) \right] \right\rangle. \tag{4}$$

In this function, μ and σ are taken in the form presented in (2). So, the likelihood function depends on the regression coefficients μ_0, σ_0, a_j, and b_j $(j = 1, 2, \cdots, J)$. They are estimated using an iterative procedure proposed by O'Neill (1971) that finds the minimum of $-\log(L)$.

b. Likelihood ratio test

Let M_1 be a model with one or more covariates. And also let l^1 and l^0 be the log likelihoods under the models M_1 and M_0, respectively. When the influence of the covariates in the model is not significant, the log likelihood ratio statistic

$$T = 2(l^1 - l^0) \tag{5}$$

is asymptotically χ_q^2 distributed (Cox and Hinkley 1974), with q being the difference in the number of free parameters in the two models. We reject hypothesis M_0 (the influences of the covariates are not statistically significant) at significance level α if T is bigger than the upper-α point of the χ_q^2 distribution. This likelihood ratio test is used to assess the statistical significance of the influence of covariates.

3. Data

a. Observation

Three types of observational data have been used in this study. They include station daily precipitation amount, gridded sea level pressure field, and humidity field for the period 1949–99. We use daily precipitation amount for North America, extracted form the Global Daily Climatology Network (Gleason 2002) compiled at the NOAA/National Climatic Data Center. We include only the stations that have at least 30 yr of complete observations during 1949–99. As a result, 4128 stations covering Canada, the United States, and Mexico are retained for this analysis. The winter season, covering the period December to March, has been selected because the influence of large-scale circulation on precipitation is strongest in the region during this season. The r in r-largest method is taken as 3; that is, we use the three largest daily precipitation amounts per

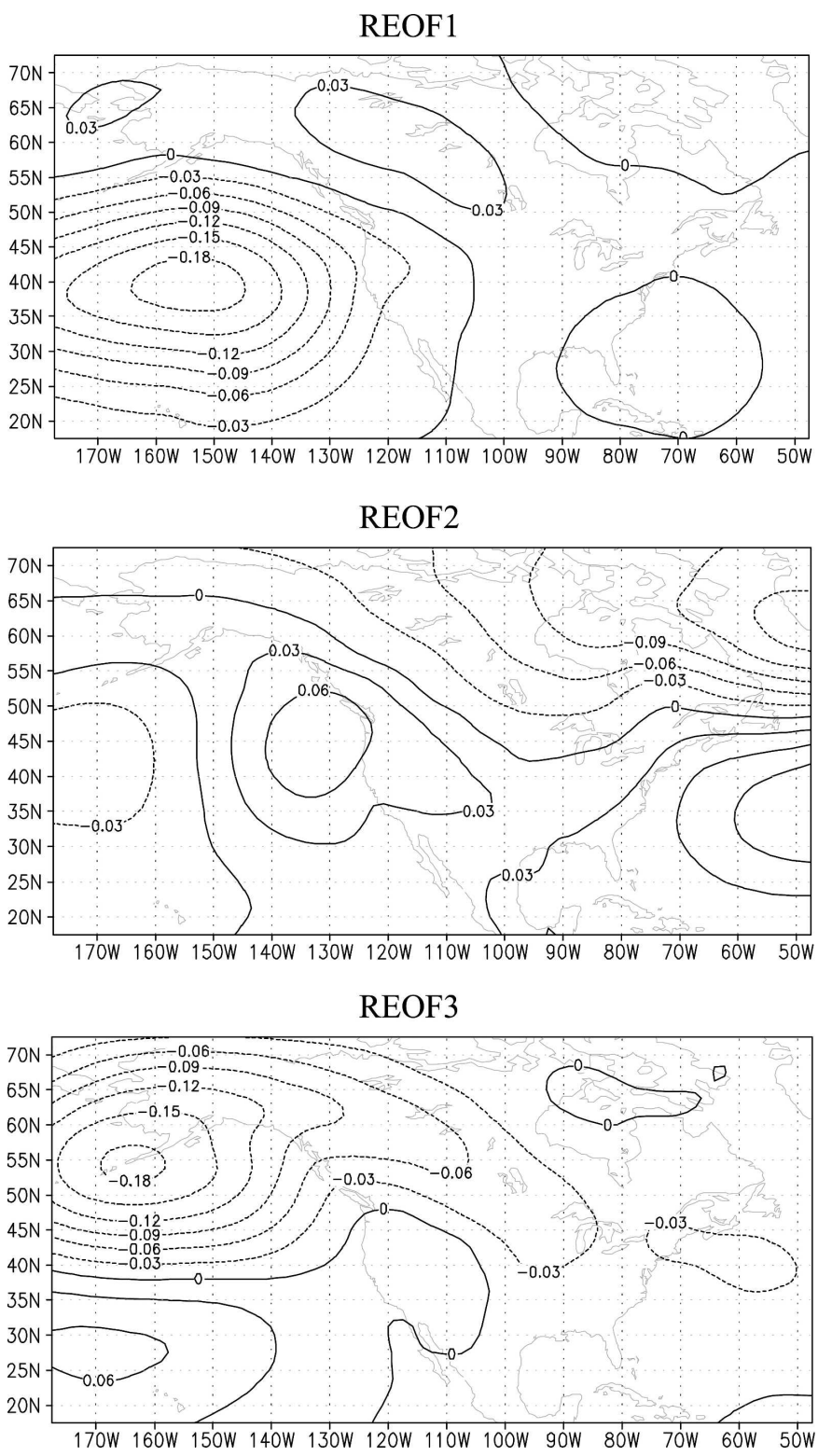

FIG. 1. The first three REOFs of observed winter sea level pressure anomalies for 1950–99.

winter as extreme daily precipitation (see Zhang et al. 2004 for details). These values are declustered so that none of the extreme daily amounts occurs within 10 days of the occurrence of another extreme precipitation (Todorovic and Zelenhasic 1970).

Gridded sea level pressure is used to represent large-scale flow patterns that influence precipitation. Though geopotential heights at 700 or 500 hPa have been frequently used to represent large-scale flow for precipitation prediction, they are not always good choices for the construction of scenarios since global warming will ultimately increase tropospheric temperatures and hence will result in higher geopotential heights (Zorita and von Storch 1999). The monthly values of the SLP field covering the eastern North Pacific and North America (15°–75°N, 180°–45°W) are extracted from the National Centers for Environmental Prediction–National Center for Atmospheric Research (NCEP–NCAR) reanalysis dataset (Kalnay et al. 1996). Winter mean SLP is computed as the average of monthly SLP through the four winter months (December to March). Wilby and Wigley (2000) showed that the maximum correlation between observed precipitation and SLP occurred at a distance away from the place of precipitation. This reflects the remote connection between SLP and station precipitation, suggesting that the large-scale flow pattern is far more important than the actual local SLP value. To preserve the large-scale flow pattern and also to keep the number of predictor variables manageable, a principal component analysis is conducted on the winter season SLP anomalies and only the leading principal components (PCs) are used as predictors. We retain the first three PCs. Each of those PCs contributes at least 10% of SLP variance. Together, they explain 73% of SLP variability. Varimax rotation is further applied on the first three leading modes. The spatial distributions of the three rotated EOFs (REOFs) are shown in Fig. 1. The first REOF is dominated by a deeper than usual lower pressure system over the North Pacific and a weak ridge over the northern part of the continent; the second REOF shows a subtropical high off the west coast and a dipole structure over the Atlantic; the third REOF displays a dipole structure too, but over the North Pacific.

The humidity-based predictor is represented by specific humidity at the 850-hPa level, which is also obtained from the NCEP reanalysis dataset. Because it is the amount of local precipitable water that plays an important role on precipitation (Wilby and Wigley 2000) at a station, the specific humidity at the station location obtained by interpolating from surrounding grids is used as the humidity predictor. The grids where humidity is employed are displayed in Fig. 2.

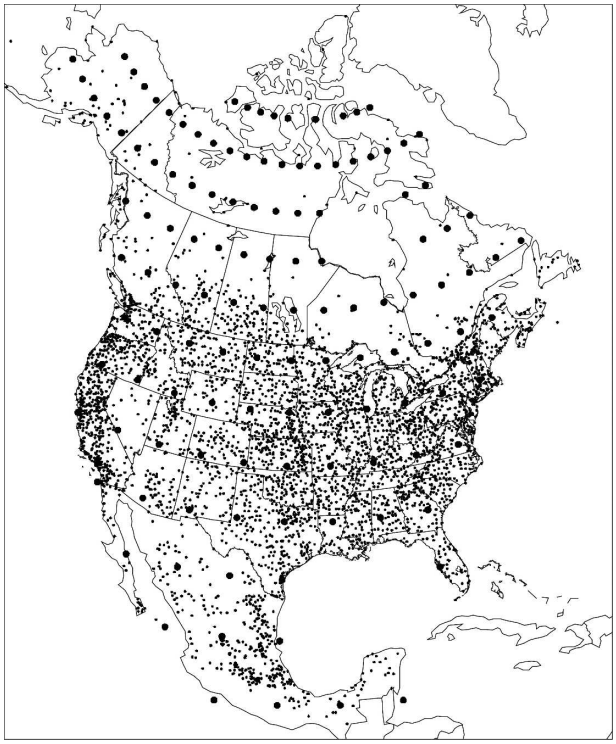

FIG. 2. Location of precipitation stations (small dots) and grid points (big dots) at which specific humidity values at the 850-hPa level are employed.

b. GCM-simulated data

Historical and future scenario simulations of sea level pressure, humidity, and precipitation conducted with the third version of the Canadian Centre for Climate Modelling and Analysis (CCCma) Coupled Global Climate Model, version 3.1 (CGCM3.1) have also been used. Flato and Boer (2001) and Scinocca and McFarlane (2004) provide some details about the model. CGCM3.1 was run at two different resolutions (T47 and T63). The T47 runs have been used here since they have more than one member in the ensemble of transient climate change experiment. This T47 version has a surface grid whose spatial resolution is roughly 3.75° latitude by longitude and 31 levels in the vertical. The ocean grid shares the same land mask as the atmosphere, but there are four ocean grid cells underlying every atmospheric grid cell. Because the NCEP reanalysis and CGCM3.1 have different resolutions, we interpolate the NCEP and CGCM3.1 original grid values to a common $5° \times 5°$ grid before they are used in the analysis.

The CGCM3.1 historical climate simulation is forced with observed greenhouse gases (GHG) concentrations and with direct aerosol forcing. The future climate

simulation is forced under the Intergovernmental Panel on Climate Change (IPCC) Special Report on Emissions Scenarios (SRES) A2 (Nakicenovic and Swart 2000), in which which is a "high" level emission in SRES range. We use the time slices of the model simulation, the periods 1950–99 and 2050–99, to represent current climate and future climate under doubling greenhouse gases concentration.

There are five members of the historical ensemble simulation. We compute the 1950–99 SLP anomalies separately for each member of the ensemble by removing their relevant mean values. These SLP anomalies are also subject to the REOF analysis. The model-simulated REOFs are shown in Fig. 3. They are in close resemblance to their counterparts from the observed sea level pressure field over the region. The simulated REOF1 is very similar to the observed REOF1 (Fig. 1, top) except that there is an additional negative anomaly centered over the Atlantic. The observed REOF2 (Fig. 1, middle) is very similar to the REOF3 from simulation, and the observed REOF3 (Fig. 1, lower) is very close to simulated REOF2. Overall, the GCM was able to capture the main features of the observed large-scale circulation over the region.

Atmospheric moisture is perhaps one of the variables that is less well simulated by GCMs. Figure 4 displays climatology of the observed and simulated historical specific humidity at 850 hPa. They show essentially the same spatial pattern, but the simulated humidity field is dryer over midlatitude land areas. Figure 5 shows the future changes in the specific humidity, which increases everywhere over the continent. This agrees well with the physical understanding that higher temperature can hold more water vapor in the atmosphere (Trenberth 1999). This means that even if the GCM does not simulate humidity variability well enough and climatology of humidity accurate enough, the future changes projected by the GCM is still physically plausible and is perhaps still creditable information for the purpose of downscaling of extreme precipitation.

The GCM-simulated changes in mean sea level pressures for 1950–99 to 2050–99 are shown in Fig. 6, which indicates that the low pressure over North Pacific will be deeper and the anticyclone circulation off the west coast will be stronger. The deeper low pressure over the North Pacific is favorable to the transport of moister air to the west coast, but its effect is modulated by the intensified offshore high pressure. As the result, the circulation change would favor carrying more moisture to the north and to the west, when compared with the southwest United States and northern Mexico (Fig. 5).

Model-simulated extreme daily precipitation may also be used to directly derive changes in the risks of extreme precipitation. It should be noted however that extreme precipitation at model grid resolution may or may not be comparable with that obtained through the statistical downscaling approach, since the model grid has a size that is far larger than an area the station observation can represent. Daily CGCM3.1 precipitation data are available for the periods 1961–2000, 2046–65, and 2081–2100. They are used to represent the current and future climates, respectively. Three members of ensemble simulations are available. Data from those simulations are concatenated to increase sample size for extreme value analysis. We fit one GEV distribution for the current climate and one GEV distribution for the future scenario extreme precipitation. We then compute the return period of the current climate 20-yr return values under future climate conditions and drive the changes in the risks of extreme precipitation due to doubling greenhouse gases concentration.

4. Results

a. Influence of predictors on extreme precipitation

The influence of predictors on the location and scale parameters of extreme daily precipitation is summarized in Fig. 7. Figure 7a indicates that a southward shifted and intensified Aleutian low is associated with an increase in location parameter over the southern and central United States and eastern coast but a decrease in location parameter over continental Alaska, the northern plains, and the Ohio River valley (ORV). This finding is in general agreement with earlier studies. Lyons (1990) identified a connection between a northward shift of the high pressure ridge and wet winter months in Texas. Cavazos (1999) discussed the influence of the Aleutian low on winter precipitation in northeastern Mexico and southeastern Texas. Cayan et al. (1998) found that the anomalously low pressure south of the Aleutians contributes to the wet conditions in the southwest United States. Coleman and Rogers (2003) identified a positive correlation between North Pacific index (NPI) of sea level pressure and ORV winter precipitation. The ridge riding over the northwestern part of the continent may result in reduced precipitation over western Canada. More than 15% of stations show significant influence of the associated PC on the location parameter at the 5% level. Figure 7b suggests that the REOF2 of the SLP anomaly—which is dominated by a large positive anomaly centered west to the coast of midlatitude North America, a positive anomaly centered over the Sargasso Sea in the southeast, and a negative anomaly in the high latitude—has significant influence on the location parameters mostly in the

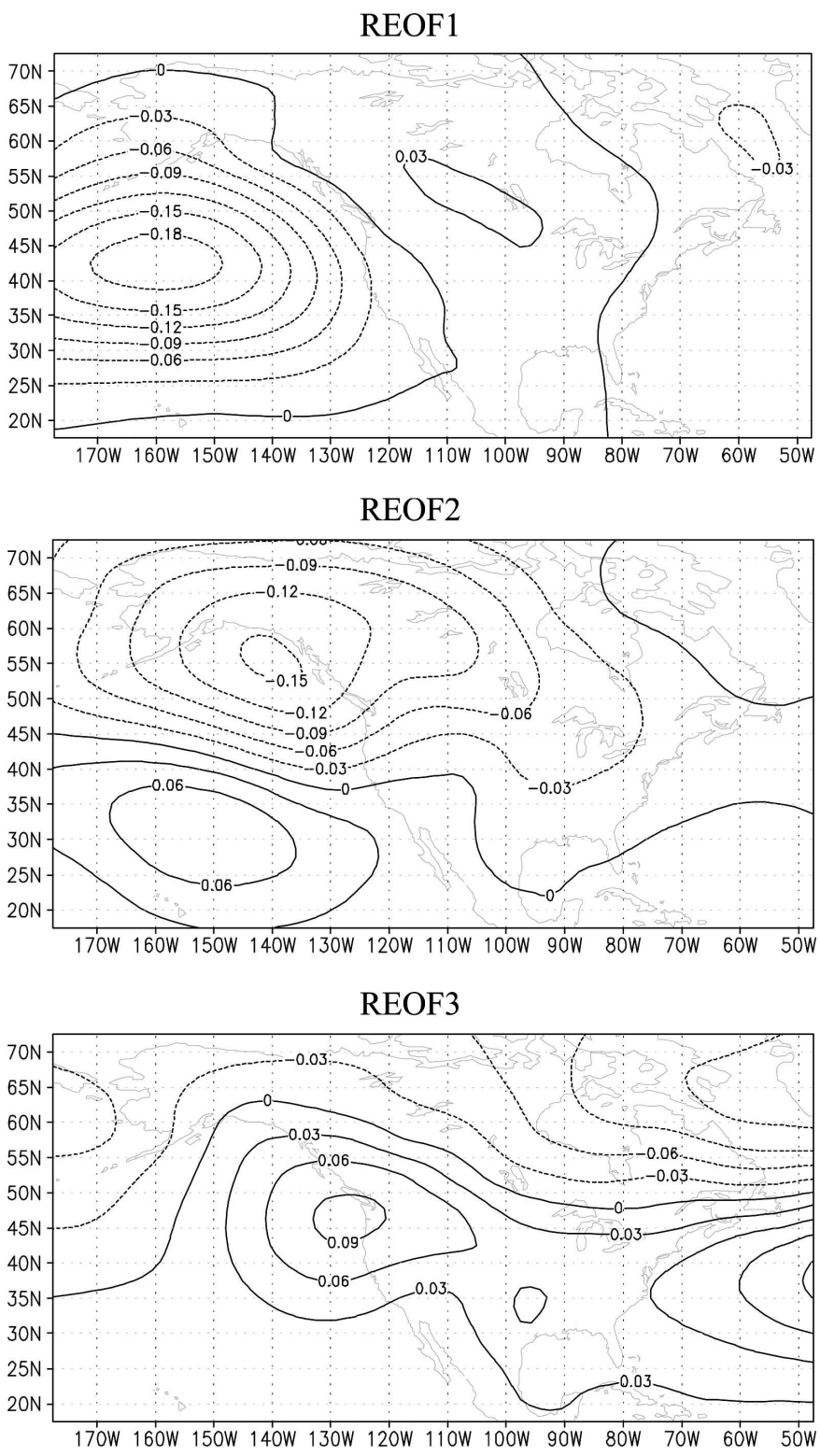

FIG. 3. The first three REOFs of model-simulated winter sea level pressure anomalies for 1950–99.

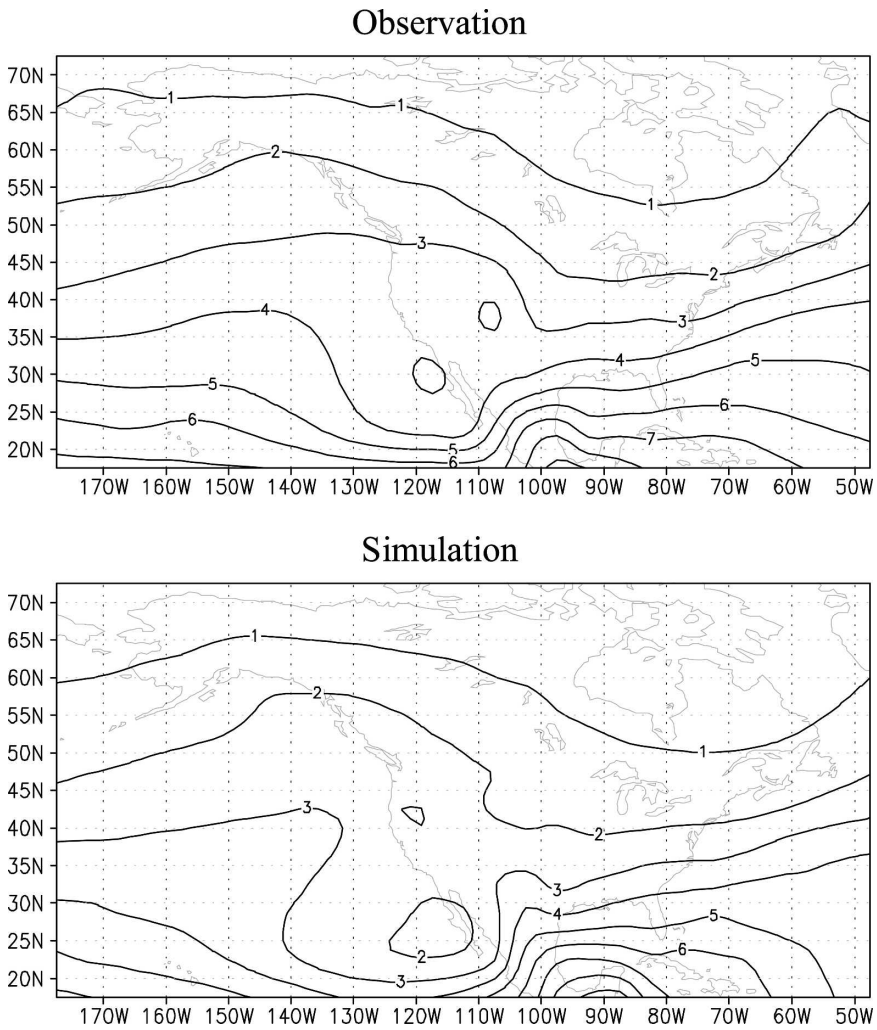

FIG. 4. 1950–99 mean specific humidity (g kg^{-1}) at the 850-hPa level from (top) NCEP reanalysis and (bottom) CGCM3.1 simulation.

western part of the continent, with lower values over the western United States, and higher values over Pacific Canada, southern Alaska, and the Great Lakes area. This is because the anticyclone circulation off the west coast brings moisture from ocean surface to the northern part of the west coast, while it plays an opposite role along southern west coast. Cayan and Peterson (1989) studied the correlation between the circulation pattern very similar to that of REOF2 and winter streamflow. They found that the high pressure centered off the coast reduces streamflow along the west coast corridor. They also found that negative streamflow anomalies in the interior are associated with a negative SLP anomaly stationed remotely over the central North Pacific. Because changes in precipitation are in good agreement with changes in the streamflow over this region (Cayan et al. 1998), this pattern of circulation would result in precipitation changes in a similar manner. The response of precipitation in the Great Lakes area to such a circulation pattern is consistent with the study of Rodionov (1994). Location parameters at about 13.8% of all stations are significantly influenced by changes associated with this pattern. The REOF3 has no significant impact on location parameter. None of the REOFs analyzed showed significant influence on the scale parameter.

Figures 7c and 7d display the connection between the specific humidity at the 850-hPa and the location and scale parameters, respectively, of the extreme precipitation distribution. The influence of humidity is significant at the 5% level at 33.6% of stations for the location parameter and at 11% of stations for the scale parameter. In general, higher humidity levels are associated with higher values of both location and scale param-

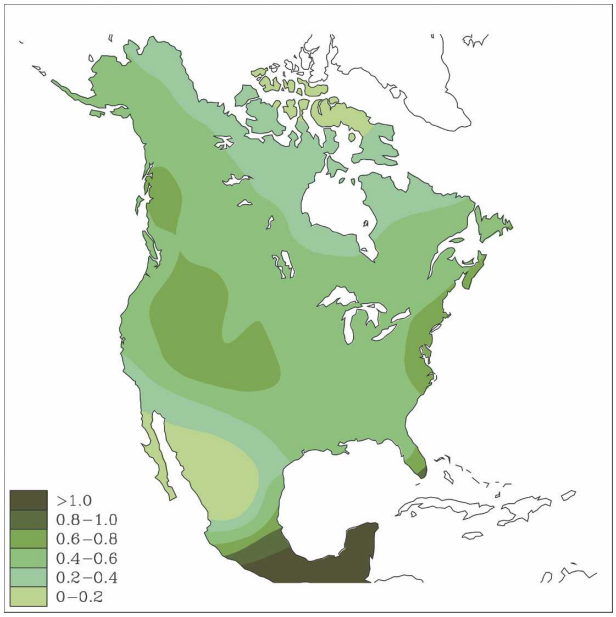

FIG. 5. CGCM3.1 projected increase in 850-hPa level specific humidity (g kg^{-1}) from 1950–99 to 2050–99.

eters, indicating that higher humidity is responsible for severe extreme precipitation. However, higher humidity may be associated with smaller location parameters, though not very significant statistically, over the northern plains and Canadian prairies. This may indicate that higher humidity levels in that region are associated with large-scale circulation that is unfavorable for precipitation in the region and that the influence of circulation overwhelms that of humidity.

The above analysis suggests that the first two leading rotated PCs of SLP and the specific humidity at the 850-hPa level should be incorporated into model fitting as covariates, with rotated PCs as covariates for the location parameter only, and humidity as a covariate for both location and scale parameters. In the following section, we show the performance of this model.

b. Statistical model validation

It is important to evaluate the skill of a statistical downscaling procedure before applying it to construct future scenarios. As the main objective of statistical downscaling is to construct scenarios for the future, and also as future climate could be quite different from the current climate, a statistical downscaling procedure needs to show skills when validated under a climate that is different from the climate under which the model is calibrated. The well-known shift in the large-scale circulation over the Northern Hemisphere, and the northern Pacific in particular, around 1976 (Trenberth 1990) provides a good testing bed for our procedure. To assess the skill of the downscaling procedure, we divide the observational data into two periods, 1949–76 and 1977–99. When compared with 1949–76, the mean sea level pressures over ocean are much lower for 1977–99, while they are higher over land. The difference could also be seen in the mean humidity values: they are higher in the west, but lower in the east (Fig. 8).

Stations in Mexico and Alaska with at least 45 yr of data, and stations in the rest of the region without missing values, are selected for the purpose of validating our downscaling procedure. This results in a total of 1064 stations being selected. Extreme precipitation data are also divided into two periods, 1949–76 and 1977–99. Figure 9 shows the risk of the 1949–76 20-yr return maximum daily precipitation in the 1977–99 period. It appears that maximum daily precipitation during 1977–99 has substantially increased over some parts

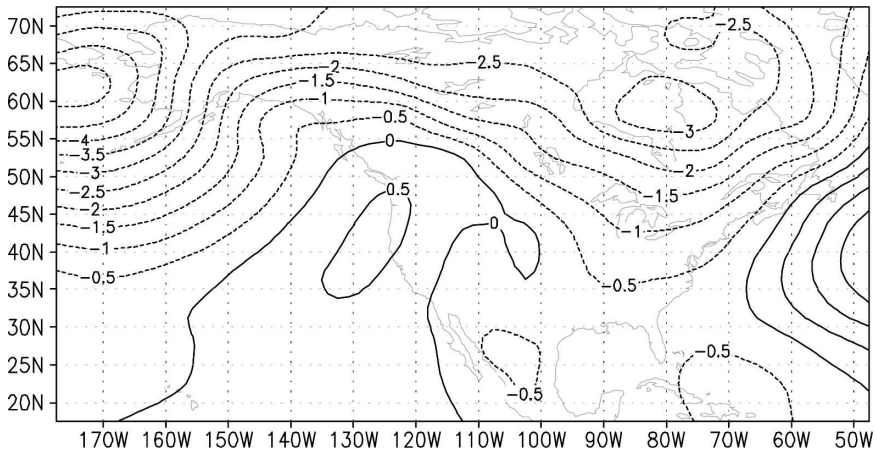

FIG. 6. CGCM3.1 projected change in sea level pressure (hPa) from 1950–99 to 2050–99.

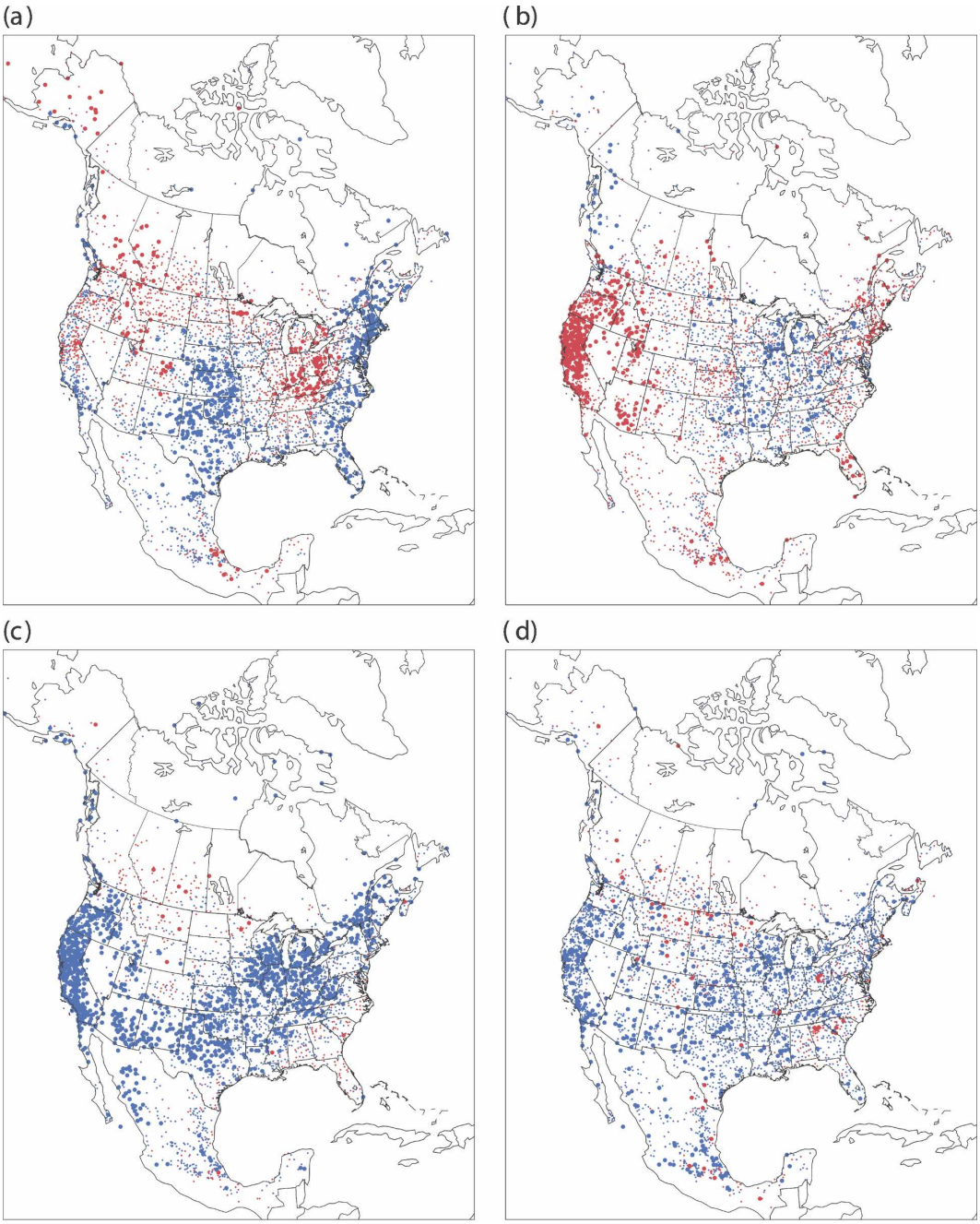

FIG. 7. (a), (b) The sign of coefficients for the first two rotated PCs of SLP on the location parameter, (c) specific humidity on the location parameter, and (d) the specific humidity on scale parameter. Blue indicates positive sign while red indicates negative sign. The bigger dots show stations whose location or scale parameters are significantly influenced by the covariates at the 5% level.

of southern United States and the west coast, but decreased over a large portion of Canada and Mexico. It should be noted that since the data density in northern Canada is very low, the pattern in this area is less reliable.

The data from one period are used to calibrate the model and data from the other period are used to validate the downscaling model. We use a skill score s defined below to evaluate the performance of the downscaling procedure:

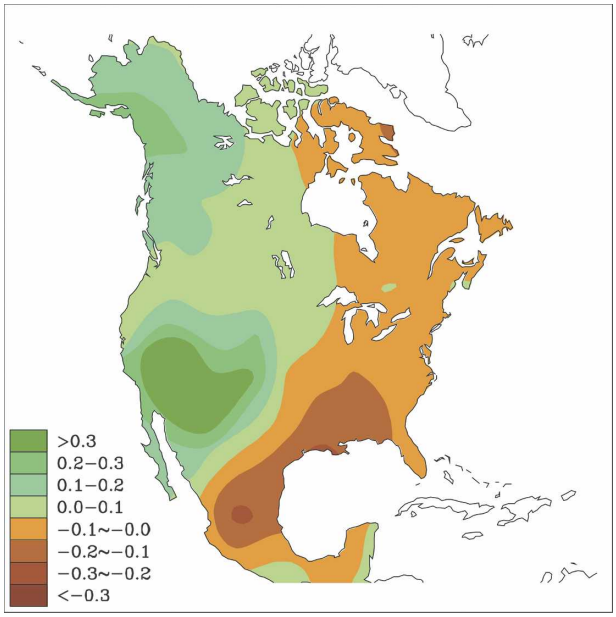

FIG. 8. Difference (g kg^{-1}) in the 850-hPa specific humidity between 1977–99 and 1949–76.

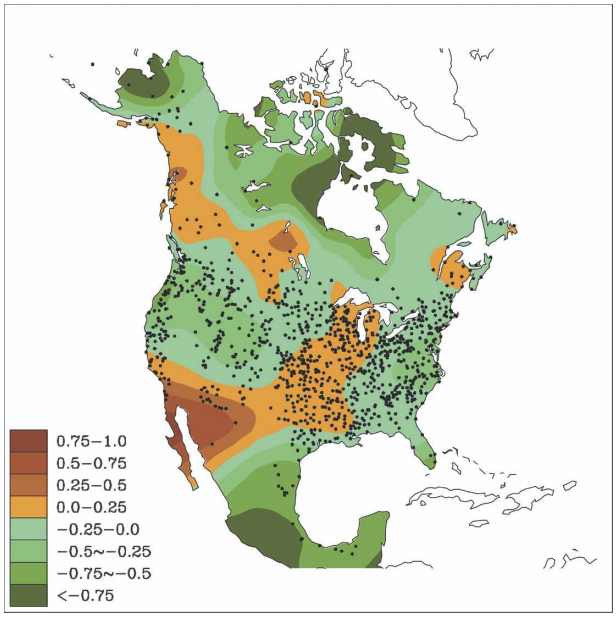

FIG. 10. The skill score s of statistical downscaling procedure in downscaling 20-yr return values of maximum daily precipitation.

$$s = 1 - |rv_d - rv_v|/|rv_c - rv_v|, \quad (6)$$

where rv_d is the downscaled 20-yr return value for the validation period, and rv_c and rv_v are observed 20-yr return values for calibration and validation periods, respectively. When the skill score s is greater than zero, that is, when the difference between the statistically downscaled return value and the observed value is smaller than the error in climate persistence forecast, the downscaling method is considered to have skill. We then interchange the data from two periods and obtain a combined score by weighting the two scores according to the period length in calibration. Figure 10 shows the map of combined skill score. The skill score is positive over northwestern Mexico, southwestern and central United States, the northwestern coast, and areas of western and eastern Canada.

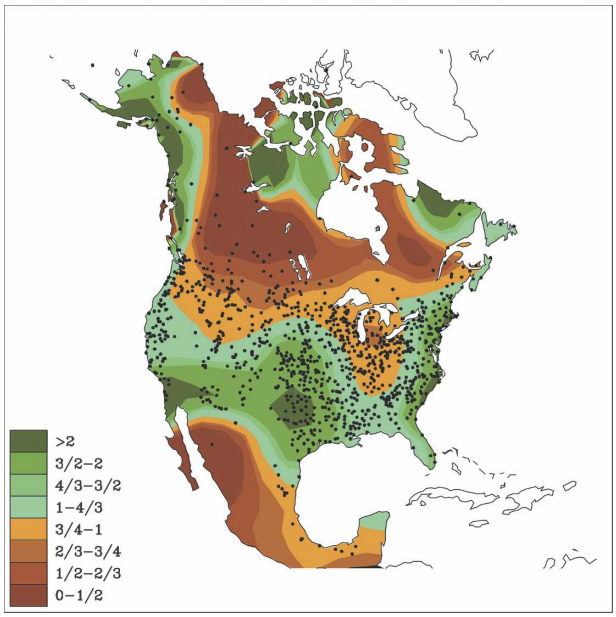

FIG. 9. The risk of 20-yr return maximum daily precipitation computed from 1949–76 during 1977–99. A value of 2 indicates that the occurrence of daily precipitation at the 20-yr return level in 1949–76 has been doubled in 1977–99. Black dots show the locations of stations.

We also computed skill score using a block bootstrap procedure. This provides some evidence of the stability of the statistical relationship. To reserve interannual variability, we divide the 50-yr observation period (1950–99) into ten 5-yr groups. Five of the groups are selected to form a 25-yr dataset for model calibration and the remaining 25-yr data for model validation. There are 252 possibilities. The skill score was originally designed for seasonal forecast for which there is usually quite a big difference between climatology and individual seasonal value. Here, we compare downscaled probability distribution with the observed one. If the difference in the probability distribution of extreme precipitation in the two datasets is small, it will be very hard for any downscaling method to improve upon the climatology. We shall therefore ask if downscaling procedure improves climate persistence forecast when the climates are different in the two periods. For this pur-

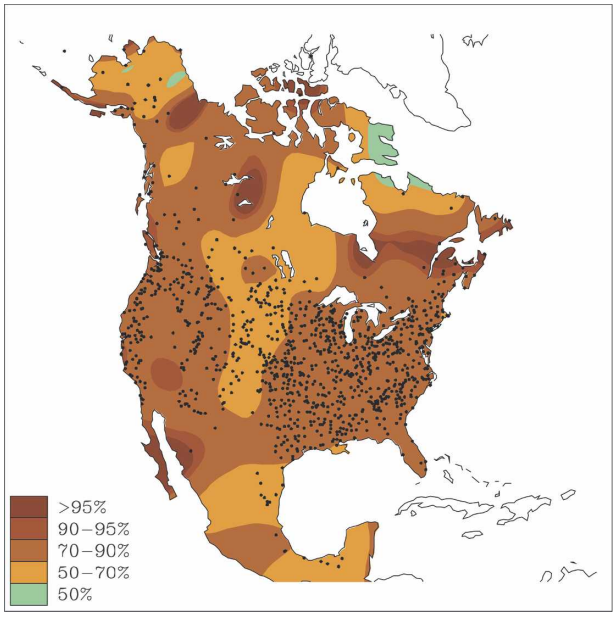

FIG. 11. The percentage of times the downscaling procedure outperforms the climate persistence forecast in 20 cases for which the difference in the mean of extremes in two subsets is largest.

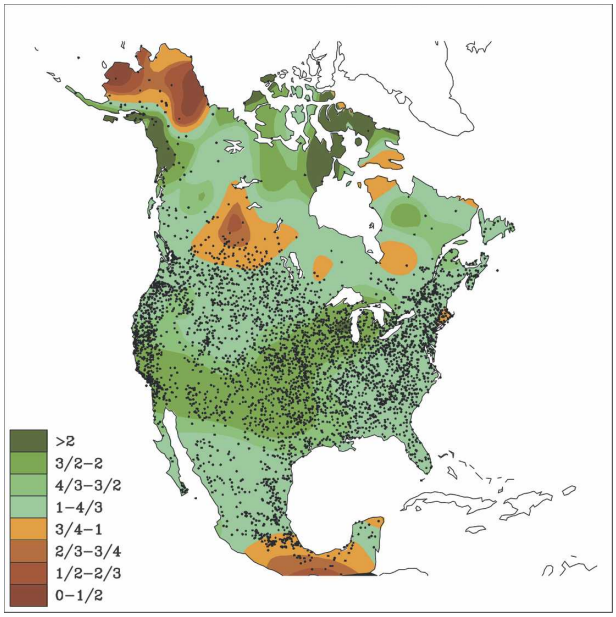

FIG. 12. Statistically downscaled changes in the risks of current 20-yr return daily precipitation in 2050–99. A value of 2 indicates that extreme daily precipitation at the 20-yr return level in current climate will occur twice as frequently in 2050–99 climate. Black dots show the locations of 4198 stations.

pose, we compute the difference in the mean values of extreme precipitation from the two subsets. We rank the absolute differences and compute the skill scores corresponding to the 20 most different subsets. Figure 11 shows the proportion of times the downscaling procedure outperforms the climate persistence forecast. It appears that our downscaling procedure improves the forecast based on climatology almost everywhere. The lower skill score shown in Fig. 10 is perhaps due to a too-small difference in the extreme precipitation during the two subperiods 1949–76 and 1977–99. These indicate that the downscaling procedure and the variations in the predictors are indeed able to capture important factors that influence extreme precipitation variation.

c. *Projected extreme precipitation change*

The observed relationships between the covariates and extreme precipitation distribution parameters are derived from the whole observational dataset at every station. They are then used to derive GEV parameters for the second half of the twenty-first century at North American stations by applying such relationships to the predictors obtained from the CGCM3.1 model simulations. The probability that the observed 20-yr return maximum daily precipitation will be exceeded in the future is then estimated. The ratio between this value and the nominal probability 0.05 represents the changes in the risks of the current 20-yr return extreme precipitation (Fig. 12). It indicates that the current 20-yr return level of daily precipitation will generally be more frequent across North America, with larger increases in the southern and central United States and the Pacific Northwest. The changes in the occurrence of 1949–99 20-yr return daily precipitation are comparable to the changes of 1949–76 20-yr return daily precipitation in 1977–99 in those regions. But this could be underestimated since the GCM may undersimulate the magnitude of anthropogenic sea level pressure change (Gillett et al. 2003). Note that lower risks in extreme precipitation appear in the Canadian prairies, in northern Alaska, and in southern Mexico. But from the northern prairies to northern Alaska, the available data are rare and our downscaling procedure does not show much skill. Therefore, our confidence of projection for these areas is low.

To understand how the changes in the large-scale circulation and the humidity contents could affect the changes in extreme precipitation, we show in Fig. 13 the projected changes in the risks attributable to changes in circulation and humidity. It appears that the changes in circulation would have an effect to reduce the risk of extreme precipitation over much of the western continent especially over the north of California, and an effect to increase the risk of precipitation in the central and eastern United States. Changes in humidity would

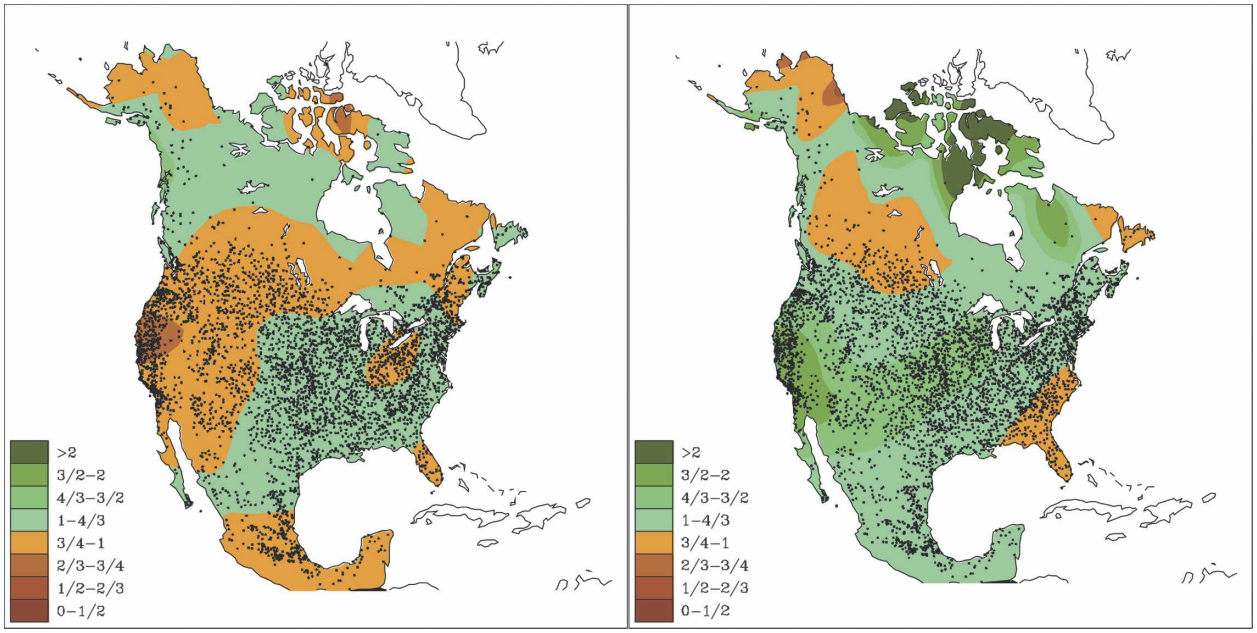

FIG. 13. Same as in Fig. 12 but for the changes in the risks that are attributable to changes in (left) large-scale circulation and (right) specific humidity separately.

result in an increase in the extreme precipitation risks in general. The pattern of projected change is more dominated by the increase in humidity.

Changes in extreme precipitation risk are also obtained from GCM-simulated daily precipitation. Because of the availability of model-simulated daily precipitation, we use the years 1961–2000 to represent current climate and years 2046–65 and 2081–2100 to represent future climate. Figure 14 shows the changes in extreme precipitation risks. It indicates an increase in the risk of extreme precipitation, at a much larger magnitude when compared with downscaling results, over much of the United States and Canada, and a strong decrease over Mexico.

Projected extreme precipitation change from the downscaling approach shows a spatial pattern similar to that obtained from GCM simulations, with richer structure and much smaller amplitude, over regions where the downscaling procedure has skill. The difference in the magnitude is perhaps due to a spatial-scale mismatch. Results from the downscaling procedure represent small scales corresponding to station locations, while those from model simulations represent areas of tens of thousands of square kilometers. The magnitude of extreme precipitation at the same return level would decrease dramatically with the increase in the spatial scale. A change in the magnitude of extreme precipitation would cause a much larger change in the risks for larger areas than for a particular location. Thus the projected changes in the extreme precipitation risks by the two approaches are broadly consistent. Because of the highly variable nature of daily precipitation both spatially and temporally, extremes observed at very large spatial scales may not be very relevant to extremes at local scales that are required for many impact

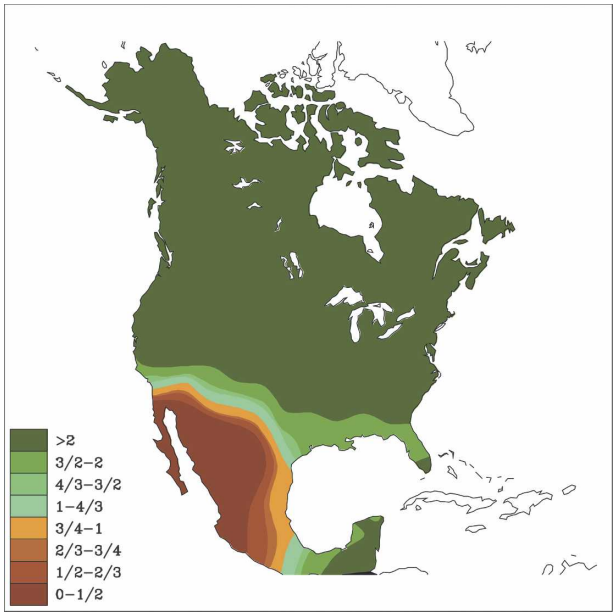

FIG. 14. Same as in Fig. 12, but computed from GCM-simulated daily precipitation.

studies. Our downscaling approach therefore does provide added value to the GCM-simulated precipitation, especially for the assessment of impacts at local scale.

The changes in the 20-yr return of winter extreme precipitation and winter mean precipitation in the GCM simulation are compared. Both show a north-increase and south-decrease contrast, almost with the same buffer zone. The increase in extremes at high and middle latitudes is stronger than that of mean precipitation, and its decrease in Mexico is less than the mean state. A difference could be seen at the southern tip of Mexico, where the extreme increases while the mean decreases. These results are consistent with the study by Groisman et al. (2005) on simulated changes in intense precipitation and mean precipitation. However, comparison between the extreme and total precipitation requires the investigation of changes in the probability distribution of total precipitation and is not discussed here.

5. Summary and discussion

By fitting generalized extreme value distributions with large-scale circulation and humidity as covariates, we have quantified the influence of those predictors on winter extreme precipitation over North America. It was found that large-scale circulation exerts a strong influence mostly on location parameters, with little impacts on scale parameter or the spread of extreme values. Different circulation patterns have impacts on different regions. Humidity has a strong impact on both location and scale parameters, which shifts the tail of the extreme precipitation distribution to the right. Performance of our downscaling method is examined with independent data under a climate condition different from the one with which the model was established. The downscaling procedure has shown useful skills.

Future changes in extreme precipitation risks at regional and local scales are derived by using the observed relationship between large-scale circulation and humidity and extreme precipitation, and projected changes in the predictor fields simulated by the CGCM3.1 model (T47) under the IPCC A2 scenario. The model projected changes in large-scale circulation and humidity would increase, due largely to the increase in the humidity field, as would the extreme precipitation risks in most parts of North America, especially in the southern and central United States and the Pacific Northwest. This agrees with Trenberth's (1999) finding that change in the atmospheric moisture content will play a large role in extreme precipitation change.

Several caveats need to be considered when interpreting the results presented in this paper. One is that, like any downscaling method, our method works only when a statistically significant relationship between predictors and predictand can be established. Future projections over the areas where the downscaling procedure showed no skill would not be reliable. The reliability of projected changes also rely on the ability of the GCM in simulating future changes in the predictors, as well as the validity of the fundamental assumption made for any statistical downscaling studies that the observed relationship would hold in the future. In addition, we only considered a linear relationship between predictors and extreme precipitation. A nonlinear relationship is possible, especially when multiple factors are considered (Jain and Lall 2001). However, consideration of a nonlinear relationship will be much more complicated. It involves making an assumption on the form of the relationship and perhaps needs more data for model estimation and validation. We only demonstrated the usefulness of our downscaling method with large-scale fields simulated by one GCM forced by one emission scenario. In real application, climate change scenarios at local scale should be produced with simulations from different GCMs under different forcing scenarios (Haylock et al. 2006).

Acknowledgments. The authors appreciate valuable comments made by Qiaobin Teng, Christoph Matulla, and Amir Shabbar. The comments from two anonymous reviewers have helped to significantly improve the paper. We thank Dave Harvey, who improved the English of the manuscript. This study was supported by Canada's Climate Change Action Fund and Canadian Foundation for Climate and Atmospheric Sciences.

REFERENCES

Bell, J. L., L. C. Sloan, and M. A. Snyder, 2004: Regional changes in extreme climatic events: A future climate scenario. *J. Climate,* **17,** 81–87.

Cavazos, T., 1999: Large-scale circulation anomalies conducive to extreme precipitation events and derivation of daily rainfall in northeastern Mexico and southeastern Texas. *J. Climate,* **12,** 1506–1523.

Cayan, D. R., and D. H. Peterson, 1989: The influence of North Pacific atmospheric circulation on streamflow in the West. *Aspects of Climate Variability in the Pacific and the Western Americas, Geophys. Monogr.,* Vol. 55, Amer. Geophys. Union, 375–397.

——, M. D. Dettinger, H. F. Diaz, and N. E. Graham, 1998: Decadal variability of precipitation over western North America. *J. Climate,* **11,** 3148–3166.

Coleman, J. S. M., and J. C. Rogers, 2003: Ohio River Valley winter moisture conditions associated with the Pacific–North America teleconnection pattern. *J. Climate,* **16,** 969–981.

Coles, S., 2001: *An Introduction to Statistical Modeling of Extreme Values*. Springer-Verlag, 208 pp.

Cox, D. R., and D. V. Hinkley, 1974: *Theoretical Statistics.* Chapman and Hall, 511 pp.

Crane, R. G., and B. C. Hewitson, 1998: Double CO_2 precipitation changes for the Susquehanna basin: Downscaling from the GENESIS general circulation model. *Int. J. Climatol.,* **18,** 65–76.

Easterling, D. R., 1999: Development of regional climate scenarios using downscaling approach. *Climatic Change,* **41,** 615–634.

Flato, G. M., and G. J. Boer, 2001: Warming asymmetry in climate change simulations. *Geophys. Res. Lett.,* **28,** 195–198.

Gillett, N. P., F. W. Zwiers, A. J. Weaver, and P. A. Stott, 2003: Detection of human influence on sea-level pressure. *Nature,* **422,** 292–294.

Gleason, B. E., 2002: National Climatic Data Center data documentation for data set 9101. Global Daily Climatology Network, version 1.0, 26 pp.

Groisman, P. Ya., and Coauthors, 1999: Changes in the probability of heavy precipitation: Important indicators of climatic change. *Climatic Change,* **42,** 243–283.

——, R. W. Knight, D. R. Easterling, T. R. Karl, G. C. Hegerl, and V. N. Razuvaev, 2005: Trends in intense precipitation in the climate record. *J. Climate,* **18,** 1326–1350.

Harpham, C., and R. L. Wilby, 2005: Multi-site downscaling of heavy daily precipitation occurrence and amounts. *J. Hydrol.,* **312,** 235–255.

Haylock, M. R., G. C. Cawley, C. Harpham, R. L. Wilby, and C. M. Goodess, 2006: Downscaling heavy precipitation over the United Kingdom: A comparison of dynamical and statistical methods and their future scenarios. *Int. J. Climatol.,* **26,** 1397–1415.

Jain, S., and U. Lall, 2001: Floods in a changing climate: Does the past represent the future? *Water Resour. Res.,* **37,** 3193–3206.

Kalnay, E., and Coauthors, 1996: The NCEP/NCAR 40-Year Reanalysis Project. *Bull. Amer. Meteor. Soc.,* **77,** 437–471.

Katz, R. W., 1999: Extreme value theory for precipitation: Sensitivity analysis for climate change. *Adv. Water Resour.,* **23,** 133–139.

——, M. B. Parlange, and P. Naveau, 2002: Statistics of extremes in hydrology. *Adv. Water Res.,* **25,** 1287–1304.

Kharin, V. V., and F. W. Zwiers, 2000: Changes in the extremes in an ensemble of transient climate simulations with a coupled atmosphere–ocean GCM. *J. Climate,* **13,** 3760–3788.

——, ——, and X. B. Zhang, 2007: Changes in temperature and precipitation extremes in the IPCC ensemble of global coupled model simulations. *J. Climate,* **20,** 1419–1444.

Lyons, S. W., 1990: Spatial and temporal variability of monthly precipitation in Texas. *Mon. Wea. Rev.,* **118,** 2634–2648.

Meehl, G. A., and Coauthors, 2000: An introduction to trends in extreme weather and climate events: Observations, socioeconomic impacts, terrestrial ecological impacts, and model projections. *Bull. Amer. Meteor. Soc.,* **81,** 413–416.

Nakicenovic, N., and R. Swart, Eds., 2000: *Special Report on Emissions Scenarios (SRES).* Cambridge University Press, 570 pp.

O'Neill, R., 1971: Algorithm AS 47: Function minimization using a Simplex procedure. *Appl. Stat.,* **20,** 338–345.

Rodionov, S. N., 1994: Association between winter precipitation and water level fluctuations in the Great Lakes and atmospheric circulation patterns. *J. Climate,* **7,** 1693–1706.

Schmidli, J., C. M. Goodess, C. Frei, M. R. Haylock, Y. Hundecha, J. Ribalaygua, and T. Schmith, 2007: Statistical and dynamical downscaling of precipitation: An evaluation and comparison of scenarios for the European Alps. *J. Geophys. Res.,* **112,** D04105, doi:10.1029/2005JD007026.

Scinocca, J. F., and N. A. McFarlane, 2004: The variability of modeled tropical precipitation. *J. Atmos. Sci.,* **61,** 1993–2015.

Smith, R. L., 1989: Extreme value analysis of environmental time series: An application to trend detection in ground-level ozone (with discussion). *Stat. Sci.,* **4,** 367–393.

Todorovic, P., and E. Zelenhasic, 1970: A stochastic model for flood analysis. *Water Resour. Res.,* **6,** 1641–1648.

Trenberth, K., 1990: Recent observed interdecadal climate changes in the Northern Hemisphere. *Bull. Amer. Meteor. Soc.,* **71,** 988–993.

——, 1999: Conceptual framework for changes of extremes of the hydrological cycle with climate change. *Climatic Change,* **42,** 327–339.

Wang, X. L., F. W. Zwiers, and V. R. Swail, 2004: North Atlantic Ocean wave climate change scenarios for the twenty-first century. *J. Climate,* **17,** 2368–2383.

Wigley, T. M. L., P. D. Jones, K. R. Briffa, and G. Smith, 1990: Obtaining sub-grid-scale information from coarse-resolution general circulation model output. *J. Geophys. Res.,* **95,** 1943–1953.

Wilby, R. L., and T. M. L. Wigley, 2000: Precipitation predictors for downscaling: Observed and general circulation model relationships. *Int. J. Climatol.,* **20,** 641–661.

Zhang, X. B., F. W. Zwiers, and G. L. Li, 2004: Monte Carlo experiments on the detection of trends in extreme values. *J. Climate,* **17,** 1945–1952.

Zorita, E., and H. von Storch, 1999: The analog method as a simple statistical downscaling technique: Comparison with more complicated methods. *J. Climate,* **12,** 2474–2489.

Zwiers, F. W., and V. V. Kharin, 1998: Changes in the extremes of climate simulated by CCC GCM2 under CO_2 doubling. *J. Climate,* **11,** 2200–2222.